Assessing the Expansion of Ground Motion Sensing Capability in Smart Cities via Internet Fiber Optic Infrastructure

Scott Anderson*[1], Erin Cunningham[1], Paul Barford[1], Dante Fratta[1], Tarje Nissen-Meyer[2], and Herb Wang[1]

1. University of Wisconsin, Madison, WI, USA, https://orcid.org/0000-0001-7785-3296 (SA) https://orcid.org/0000-0002-9680-6812 (EC) https://orcid.org/0000-0001-7874-1819 (PB) https://orcid.org/0000-0003-0478-6760 (DF) https://orcid.org/0000-0000-0000-0000 (HW) ; 2. University of Oxford, Oxford, Oxfordshire, GB, https://orcid.org/0000-0002-9051-1060 (TNM)

*Corresponding author: Scott Anderson, 1210 W. Dayton Street, Madison, WI 53706-1613, standerson4@wisc.edu

Cite this article as (2023). Assessing the Expansion of Ground Motion Sensing Capability in Smart Cities via Internet Fiber Optic Infrastructure, *Bull. Seismol. Soc. Am.* **XX**, 1–24, doi: .

Abstract

Monitoring ground motion in Smart Cities can improve public safety by providing critical insights on natural and anthropogenic hazards *e.g.,* earthquakes, landslides, explosions, infrastructure failures, etc. Although seismic activity is typically measured using dedicated point sensors (*e.g.,* geophones and accelerometers), techniques such as Distributed Acoustic Sensing (DAS) have demonstrated the utility of using fiber optic cable to detect seismic activity over longer distances. In this paper we present results of a study that quantifies the expansion in area monitored for low-amplitude ground motion events by augmenting existing point sensors with Internet fiber optic cable infrastructure. We begin by describing our methodology, which utilizes geospatial data on point sensors and Internet optical fiber deployed in Metropolitan Statistical Areas (MSAs) in the US. We extend these data to identify the area that can be monitored by *(i)* considering observed seismic noise data in target locations, *(ii)* modifying the model by Wilson et al. (2021) for applicability to optical fiber sensing and *(iii)* optimizing selection of fiber segments to maximize coverage and minimize deployment costs. We implement our methodology in ArcGIS to assess the additional area that can be monitored for low-amplitude ground motion events (*i.e.,* > magnitude 0.5) by utilizing Internet fiber optic cables in the 100 largest MSAs in the US. We find that the addition of Internet fiber-based sensors in MSA's would increase the area monitored on average by over an order of magnitude from 1% to 12% if min/max fiber is used and 20% if all fiber is used.

INTRODUCTION

Large scale monitoring of ground motion has many applications in smart cities[1], including public safety, transportation, and industrial activity. To monitor ground motion, individual sensors are typically placed in target locations to measure phenomena of interest such as earthquakes or infrastructure movement. These sensors are selected to monitor specific amplitudes and frequency ranges of ground motion. Two of the most important considerations in sensor selection are sensitivity and cost. A high-end permanent broadband seismic station whose low-frequency sensitivity extends to less than 0.01 Hz can cost upwards of $16,000 Krokidis et al. (2022). Additionally, each sensor must include security, power, and communications infrastructure to relay data streams back to a central facility for processing, analysis, and storage. An inherent limitation of these sensors is the area over which they can effectively detect motion, which is determined by various factors including their sensitivity and background noise in the location of their deployment.

Scientists and governments have deployed networks of ground motion sensors worldwide to monitor seismic activity. These networks of sensors are densely deployed in areas of active tectonic movement. Conversely, commercial organizations deploy networks of sensors for activities such as oil and natural gas exploration, or monitoring mining activities. Deployments of these networks of sensors are in targeted locations, typically not in metropolitan areas. While data from

[1] For this research, we define a *Smart City* as a city that leverages the collection, processing, analysis, and use of data from distributed sensors placed throughout the urban infrastructure to enable effective city governance and function in diverse areas of public interest, *e.g.,* mobility, economy, and facilities management Kirimtat et al. (2020).

scientific and government-sponsored seismic networks are often publicly available, data from commercial seismic networks are private. Thus, existing networks of ground motion sensors may not be sufficient to monitor metropolitan areas for smart city applications.

New methodologies for ground motion sensing using infrastructure that is already in place offer opportunities to lower costs and expand coverage in smart cities. One type of ground motion monitor that has been proposed includes the use of accelerometers on mobile phones Reilly et al. (2013). While this approach is technically feasible, it requires users to install an app on their phone, and raises privacy concerns since an individual's location and activities would be monitored. Another approach is based on deployment of fiber optic cable. Multiple studies have demonstrated the feasibility of using fiber optic cable to monitor activities and events such as passing traffic or earthquakes Shen and Zhu (2021); Lindsey et al. (2020); Ajo-Franklin et al. (2019). Most of these studies use a technique called Distributed Acoustic Sensing (DAS), which can be deployed on existing telecommunications fiber optic infrastructure without interrupting standard data transmissions Martin et al. (2017); Zhu et al. (2021). A significant advantage of DAS versus traditional sensors is that it enables sensing *along the entire length of a fiber with a spatial resolution of a few meters*, thus dramatically increasing the sensor density and area that can be monitored. Although DAS has been shown to be a highly effective sensing technology and fiber optic cables are already densely deployed in metropolitan areas (thus alleviating the need to install new infrastructure), the question remains of how to quantify the expansion of the monitored area by augmenting existing ground motion sensing arrays with fiber optic cable-based sensor networks in smart cities. Our objective in this study is to address this question.

We propose a methodology for assessing the expansion of monitored area by deploying ground motion sensing capabilities along the fewest existing fiber optic cables to augment sensing capabilities in smart cities. Identifying the fewest number of fiber segments that provide the largest new coverage area is critical to the economic success of large-scale deployments of ground motion sensing on fiber optic cables. Considerations for this sensing strategy include the cost of DAS sensors (which are currently about 10x the cost of traditional point sensors) and the amount of data that must be processed. By identifying the fewest new fiber segments that require sensing capabilities, we minimize the cost to deploy this capability, as well as the amount of data that must be processed and stored.

Our methodology uses a geographic information system (GIS) to spatially analyze maps of metropolitan areas, locations of dedicated seismic sensors, and deployed fiber optic cable. Specifically, we use GIS to spatially analyze these different information layers and quantify the spatial relationship of sensor coverage area from existing seismic sensors augmented by sensors deployed on fiber optic cable.

We first gathered location information for metropolitan areas in the United States, existing networks of seismic sensors, as well as operational fiber optic cable in the US. We extended this information with noise levels observed at existing seismic sensors to calculate sensing coverage areas. We use the model by Wilson *et al.* to map noise levels observed at each sensor to identify detection threshold ranges, *i.e.,* the area around a sensor in which a ground motion event could be detected above background noise levels without human interpretation Wilson et al. (2021). In this research, we consider detection areas for ground motion events with magnitude M0.5 (*i.e.,* very small events such as trains passing) and higher. (Earthquakes are measured by magnitude (M), which describes the size of the earthquake based on physical characteristics of the emitted waveforms USGS Earthquake Hazards Program (2023).) For comparison, a M1.0 earthquake is roughly comparable to an explosion of 70 pounds of TNT (mid-sized construction blast) and a M2.0 earthquake is approximately equivalent to an explosion of 1 metric ton of TNT Observatory (2008). We also applied this technique to linearly distributed sensors, such as those that could be constructed by deploying DAS on existing fiber optic infrastructure. Finally, we determined the optimal deployment of ground motion sensors on existing fiber infrastructure to maximize the coverage area while using the fewest number of fiber optic cable segments.

We utilize our technique to assess combinations of existing dedicated seismic sensors and hypothetical arrays of sensors based on existing fiber optic cable in the 100 largest MSAs (by population). Our analysis shows that there are an average of three seismic point sensors currently deployed in each MSA. On average, these seismic sensors can detect ground motion events of magnitude M0.5 in about 1% of an MSA's area. In contrast, we find that if all fiber optic cable in each MSA were used as sensors, on average, low magnitude ground motion events could be detected in 19% of the MSA total area. We also find that if both existing point sensors and sensors deployed on all fiber optic cables were utilized in an MSA, on average, low-magnitude events could be detected in 2,200 km^2 (20%) of an MSA's total area. Finally, using an optimal selection technique to limit the number of fiber optic cable segments required, on average we find that 1,400 km^2 (12%) of each MSA could be covered by either a fiber optic sensor or an existing seismic sensor.

We highlight the details revealed by our technique through specific examples of the spatial relationships for the Little Rock, AR and Seattle, WA MSAs. These examples allow us to visualize the sensor coverage areas when existing point sensors and sensors deployed on fiber optic cables provide complementary coverage. We also use these MSAs to demonstrate the utility of the optimal deployment strategy by showing how many fiber optic cable segments overlap and how we can still obtain significantly better coverage using a limited number of new sensors deployed on fiber optic cable.

RELATED WORK

This research benefits from previous work in several different areas of study, including smart cities, ground motion sensing, distributed acoustic sensing (DAS), Internet Photonic Sensing, and GIS-informed sensor placement.

Our study is inspired by the idea of the smart city. Smart cities are urban areas that use technology and data from distributed sensors to enable effective city governance and improve quality of life in diverse areas of public interest, *e.g.,* increase efficiency, improve sustainability, or reduce costs. Technology use often includes using sensors and Internet-connected devices to monitor and manage vehicular traffic Rizwan et al. (2016), energy use Mahapatra et al. (2017), waste Nirde et al. (2017); Aazam et al. (2016), and infrastructure health Adedeji et al. (2022), as well as using data analytics to improve decisionmaking and public services D'Aniello et al. (2020). Related research explores using smartphones to detect seismic activity for early warning systems Kong et al. (2016). Although previous studies have identified many different benefits from using Internet-connected devices and sensors for a variety of use cases in cities, none have attempted to quantify the extent of which currently-deployed Internet infrastructure could be used to improve the ability to understand urban area activities.

Ground motion sensing refers to the measurement of the time history of ground vibration. This type of measurement includes sensing of earthquakes, construction and mining activities, and subsidence or slope failure. Measurements of these motions are taken by a variety of types of sensors. The United States Geological Survey (USGS) typically uses three types of sensors as components of the Advanced National Seismic System (ANSS): broadband, short-period, and strong-motion sensors Working Group on Instrumentation, Siting, Installation, and Site Metadata (2008). Broadband sensors measure seismic motions with wide frequency and amplitude limits. Short-period sensors have limited bandwidth and are typically limited to frequencies above ∼1 Hz. Strong-motion sensors measure large amplitude motions. In addition to sensors used as part of national and regional networks, studies have shown that micro-electromechanical system (MEMS) accelerometers may be used as lower-cost seismic sensors Fu et al. (2019); Cascone et al. (2021). The point-sensors typically used in seismic monitoring networks are widely deployed and our study seeks to understand how their monitoring capacity could be augmented to detect low-magnitude events in smart cities using linear sensors based on deployed Internet fiber optic cable.

In addition to using dedicated seismic sensors, many researchers have proposed using fiber optic cable to detect ground motion events. This is argued to be especially useful in areas where traditional seismic sensor deployment may prove difficult, such as metropolitan areas. One such technique is Distributed Acoustic Sensing (DAS) Parker et al. (2014); Lindsey et al. (2017). DAS uses fiber optic cables as sensors to detect, locate and measure acoustic waves along the length of a cable. The technology works by sending rapid pulses of laser light at regular intervals and then measuring the Rayleigh backscattered light using a photodiode that is co-located with the laser. Disturbances in the fiber such as acoustic waves, temperature changes, and mechanical vibrations create small changes in the properties of the fiber that can be detected and converted into measurements of strain along a cable.[2] In addition to DAS, which commonly uses dedicated fiber optic cable, Internet Photonic Sensing (IPS) has been proposed to use existing fiber optic cable from Internet Service Provider (ISP) networks Patnaik et al. (2021). Whereas DAS requires a dedicated interrogator unit to be deployed, IPS proposes utilizing existing Internet transport hardware to detect strain on fiber. Both DAS and IPS demonstrate that it is possible to use a fiber optic cable as a ground motion sensor. Additional research showed the possibility of using existing fiber optic cable in urban areas as a component of the smart city Zhu et al. (2021). Our research provides a quantitative analysis of how far sensor networks' range could be extended when complemented by ground motion sensors deployed on existing ISP networks.

Finally, our work is informed by prior studies that have utilized GIS to consider how to distribute sensors for monitoring applications. The problem of geosensor deployment for environmental monitoring has been addressed in a number of prior

[2] This is similar to optical time-domain reflectometry (OTDR), which is commonly used to detect and locate faults in optical fiber but does not detect strain.

studies. Argany *et al.* present a survey of techniques for optimized geosensor network deployment that are based on utilizing Voronoi diagrams and Delaunay triangulation Argany et al. (2011). More recently, a smart city-related study considered how to utilize GIS in conjunction with data from structural sensors to assess the integrity of bridges in areas of seismic activity Malekloo et al. (2020). While these studies provide useful perspective, we are not aware of any prior work that considers how GIS can be used to assess the expansion of ground motion monitoring via Internet fiber infrastructure.

DATASETS

To conduct our study, we utilized multiple data sources on the spatial extent of metropolitan areas, Internet fiber optic cable, and existing ground motion sensors. We analyzed these data sets as spatial layers using GIS to assess the extent to which ground motion sensing capability can be expanded via existing fiber infrastructure.

To capture the spatial extent of metropolitan areas, we used the US Census Bureau Cartographic Boundary Files United States Census Bureau (2023). These digital boundary files provide spatial limits for various geographic areas, including states, counties, census tracts, and block groups for the United States. These files are designed to be used with GIS software and other mapping programs for spatial analysis. Because of our interest in smart cities, we used the Metropolitan Statistical Area (MSA) shapefiles, which encompass city administrative boundaries as well as the surrounding area that is economically and culturally similar to the central metropolitan area. Note that this design choice leads to conservative results on expanded coverage for smart cities since in most cases MSA boundaries extend beyond city limits.

For a spatial understanding of in-use ISP fiber optic cable infrastructure, we used the Internet Atlas metropolitan fiber optic cable shapefiles Durairajan et al. (2013). Internet Atlas was a research project that aimed to map the physical infrastructure of the Internet, including points of presence (PoPs), fiber optic cable, and other key components of Internet physical infrastructure. This information improves the understanding of the Internet's topology and to identify potential bottlenecks and vulnerabilities. Internet Atlas includes metro fiber maps for the top 100 MSAs considered in our study (except Honolulu, HI). While these maps cannot be guaranteed to be complete, they are the most accurate source of shapefiles of metro fiber infrastructure deployment that is openly available for research.

Finally, we obtained the locations of ground motion sensors from the Incorporated Research Institutions for Seismology (IRIS) database, which includes data from seismographic stations around the world IRIS Consortium (2023). The map displays the locations of seismographic stations that are part of the IRIS Global Seismographic Network (GSN), as well as stations that are operated by other organizations. The database includes access to additional information about specific seismographic stations, such as the types of instruments that are installed, real-time data from the stations, noise data, as well as historical data.

METHODOLOGY

To assess how seismic sensing coverage can be extended by deploying sensors on Internet optical fiber in smart cities, our methodology uses ArcGIS and GeoPandas to process multiple layers of geospatial data Esri (2020); GeoPandas (2023). In the following sections, we describe our methodology in detail.

Data collection

As described in Section Datasets, we directly accessed MSA boundary and fiber optic cable shapefiles. MSA boundaries are stored as multi-polygon shapes in the MSA boundary shapefile, which also includes administrative information such as MSA name and population. The fiber optic cable shapefile included all known fiber optic cable in the US from Internet Atlas, stored as line shapes. Although the fiber optic cable shapefiles accurately describe the spatial layout of fiber optic cables, they do not necessarily reflect which cable segments were physically connected. The fiber optic shapefiles also do not include administrative information such as the ISP name. While the Internet Atlas study originated to elucidate the physical connectivity in the Internet, new, focused studies on using fiber optic cable for ground motion sensing could show deployment characteristics relevant to using fiber as a sensor, such as: *(i)* how actual fiber routes diverge from cable maps, *(ii)* locations of fiber slack loops, and *(iii)* observed noise on each segment Cunningham et al. (2022).

In contrast, we had to process information about sensor locations and noise to make it spatially relevant to the MSA and fiber location information. We first downloaded seismic sensor names, networks, and locations (lat/long) for sensors in the United States from the IRIS Gmap. This information included sensors that were no longer active as well as sensors that were planned for future deployment. We processed this data to limit our results to active sensors then used GeoPandas to process the flat lat/long coordinates into geospatial point shapes. Additionally, for each seismic sensor, we required seismic noise data. Because we considered hundreds of seismic sensors across the entire US, we collected noise information for each sensor of interest for a 24 hour period, 14 June 2022, a typical Tuesday without global large magnitude earthquakes. Noise information is provided for the three spatial components: north-south, east-west, and up-down (z) for discrete frequencies in the range of 0.005 Hz to 50 Hz. Specifically, we collected noise measurements from broad band and high broad band, high gain seismometers in the vertical (Z) orientation. Different types of sensors are sensitive to different frequency ranges, we therefore limited our analysis to a narrow band around 10 Hz, a common frequency across sensor types and low enough to be emitted by low-magnitude seismic events.

We focused on ground motion events that occur at about 10 Hz for multiple reasons. This frequency is common to all broad band and high broad band seismic sensors. Ground motion events produce seismic waves at many different frequencies. The events that we are most interested in for smart cities, such as regional seismic activity, transportation, industrial, or economic activities will produce very low magnitude ground motion signatures. These low magnitude ground motion events will produce seismic waves at low frequencies, such as 10 Hz.

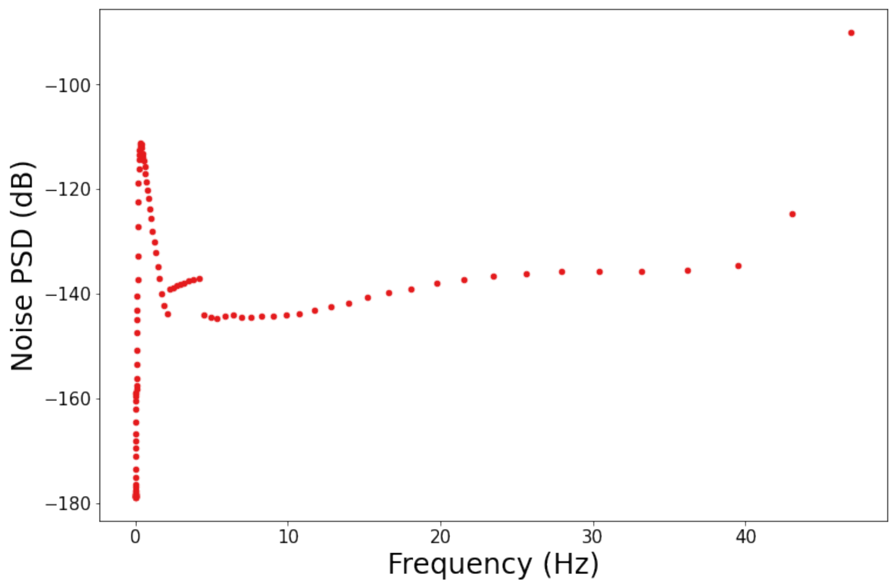

Figure 1: Observed noise on 14 June 2022 across frequencies at the Baber Butte, OR seismic sensing station (BABR).

Calculating detection threshold

With the noise data collected for each point sensor, we calculate the automatic detection threshold using the technique from Wilson et al. (2021), which we describe briefly here. Wilson *et al.* noted that the automatic detection threshold for seismic sensors varies based on the observed noise levels (which can vary greatly among different sensors) as well as temporally at the same sensor. The *automatic detection threshold* refers to the lowest magnitude seismic event that is sufficiently above the noise floor for algorithmic identification.

From their empirical study of historical events and background noise levels, Wilson *et al.* developed a model that took as input the background noise at a sensor as well as a user-provided distance from the sensor to predict the lowest magnitude event that could be detected at that distance. We reproduced these equations in 1, 2, and 3, where R is distance from sensor (in km), M is the detectable magnitude, and N is the sensor noise level (in dB).

$$if\ R < r_1 : M = a_1 log_{10}(R) + b_1 R + dN + c \tag{1}$$

$$\begin{aligned} if\ r_1 < R < r_2 : M = a_2 log_{10}(R/R_1) + a_1 log_{10}(r_1) + \\ b_2(R - r_1) + b_1 r_1 + dN + c \end{aligned} \tag{2}$$

$$\begin{aligned} if\ R > r_2 : M = a_3 log_{10}(R/r_2) + a_2 log_{10}(r_2/r_1) + \\ a_1 log_{10}(r_1) + b_2(r_2 - r_1) + b_1 r_1 + dN + c \end{aligned} \tag{3}$$

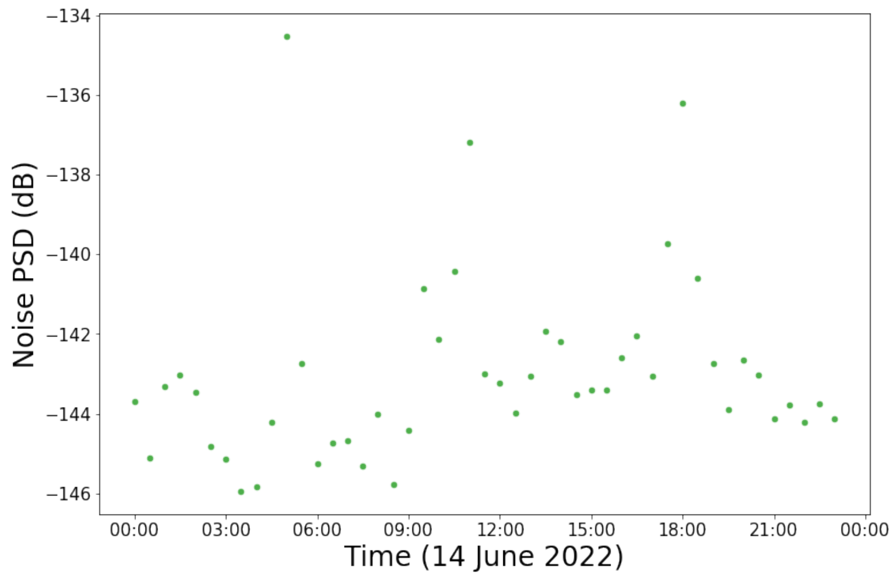

Figure 2: Observed noise on 14 June 2022 for frequency 10Hz at the Baber Butte, OR seismic sensing station (BABR).

We used the coefficients for P-waves calculated by Wilson *et al.* and reproduced in the appendix in Table 4. One limitation of our technique is that these coefficients were calculated for the central US, but we use them uniformly throughout metropolitan areas in the US. Although this is appropriate to show the feasibility of using a technique like DAS deployed on optical fiber, more regionally-aligned coefficients should be calculated and used to determine more exact detection threshold areas. In our study, we adapted these equations to determine the furthest distance that a ground motion event at a given magnitude could be detected from a given sensor.

Each sensor has distinct noise threshold characteristics in both frequency and time. Figure 1 shows an example of how noise levels vary across frequencies for a sensor at the Baber Butte, OR seismic sensing station (BABR), while Figure 2 shows how noise varies across a 24 hour period. Note that these two patterns are not necessarily representative for all sensors. Similar to Figure 1, many sensors have a frequency for which the noise is lowest. However, in contrast to Figure 2, the lowest recorded noise levels for some sensors occur during periods of minimal anthropogenic activity *i.e.,* at night. Because the noise levels vary, we calculated the average noise level over a 24 hour period for each sensor. However, other aggregations of observed noise at a sensor (*e.g.* min or max) could be used for other use cases.

Ground motion events produce seismic waves in all three spatial directions (north-south, east-west, and up-down). Our methodology could be used for analysis of different types of seismic waves (*i.e.,* surface, P-waves, or S-waves) and may incorporate noise measurements from any spatial direction. For this study, we use noise measurements along the Z-axis (up-down) because P-waves have a strong vertical component. As P-waves travel faster than S-waves, they are important for seismic activity detection and early warning systems Allen et al. (2009). Using the appropriate equations to calculate detection thresholds from noise measurements, our methodology could also be applied to surface waves from shallow sources, which have greater amplitudes and longer periods than P-waves, which is useful for monitoring near-surface events.

We use the average noise and desired seismic event magnitude to calculate the radius around each sensor within which any seismic event of that magnitude or greater could be automatically detected. We use this radius to spatially generate a buffer around the sensor in a GIS. For point sensors, such as traditional seismic sensors, this buffer corresponds to a circle around the sensor. For ground motion events with magnitude greater than M2.0, the events could be detected hundreds to thousands of kilometers from a sensor. This leads to complete and overlapping coverage for most MSAs. However, lower magnitude events may be detected only when they occur much closer to a sensor. For example, the seismic sensor with the lowest average noise power spectral density (PSD) could detect M0.5 seismic events within 30 km and M1.5 events within 200 km. On average, a sensor could detect M0.5 events out to 2.3 km and M1.5 events within 65 km of the sensor. We assume that detection thresholds around a sensor are uniform, *i.e.,* they form a circle around the sensor within which all seismic events of that magnitude or greater could be detected.

To compare the detection coverage of dedicated seismic sensors to sensors using fiber optic cable, we must develop a convention for the detection threshold of fiber optic cable. One consideration for the detection threshold is the directional sensitivity of DAS. In particular, DAS is sensitive to axial strain on a fiber, so deliberately placed DAS arrays often use specific geometric arrangements of the fiber optic cable Wuestefeld and Wilks (2019); Wang et al. (2018). Although existing fiber optic cable does not necessarily follow the same geometric patterns as a deliberately placed DAS array, it is often run in a multi-directional pattern which would provide complete coverage around the fiber segments. We do not have a source of real-world noise measurements from ground motion sensors currently deployed on fiber optic cable, but we make the assumption that these sensors would not be well-placed for ground motion detection and would therefore be susceptible to high noise levels. As a conservative estimate for the detection threshold of sensors in fiber optic cable, we use 1.5 km for events of M0.5 or greater, which is well below the average detection threshold for dedicated seismic sensors. We anticipate refining this estimate with future sensor deployments using fiber optic cables, including the ability to measure individual noise levels for different fiber optic cable segments.

We concentrate on M0.5 events for our analysis because seismic sensors are geographically widespread enough to detect events of larger magnitude, and the anthropogenic events we focus on in smart cities will only produce very low magnitude ground motion. However, our methodology is robust enough to be applied for smaller or larger magnitude events as desired.

Detection threshold buffers around point sensors are uniform circles of radius *detection threshold distance* with the sensor as the center of the circle. In contrast, for linearly distributed sensors based on fiber optic cables, the detection threshold buffer is an irregular polygon enclosing the linear sensor in which the polygon edge is *detection threshold distance* from the linear sensor.

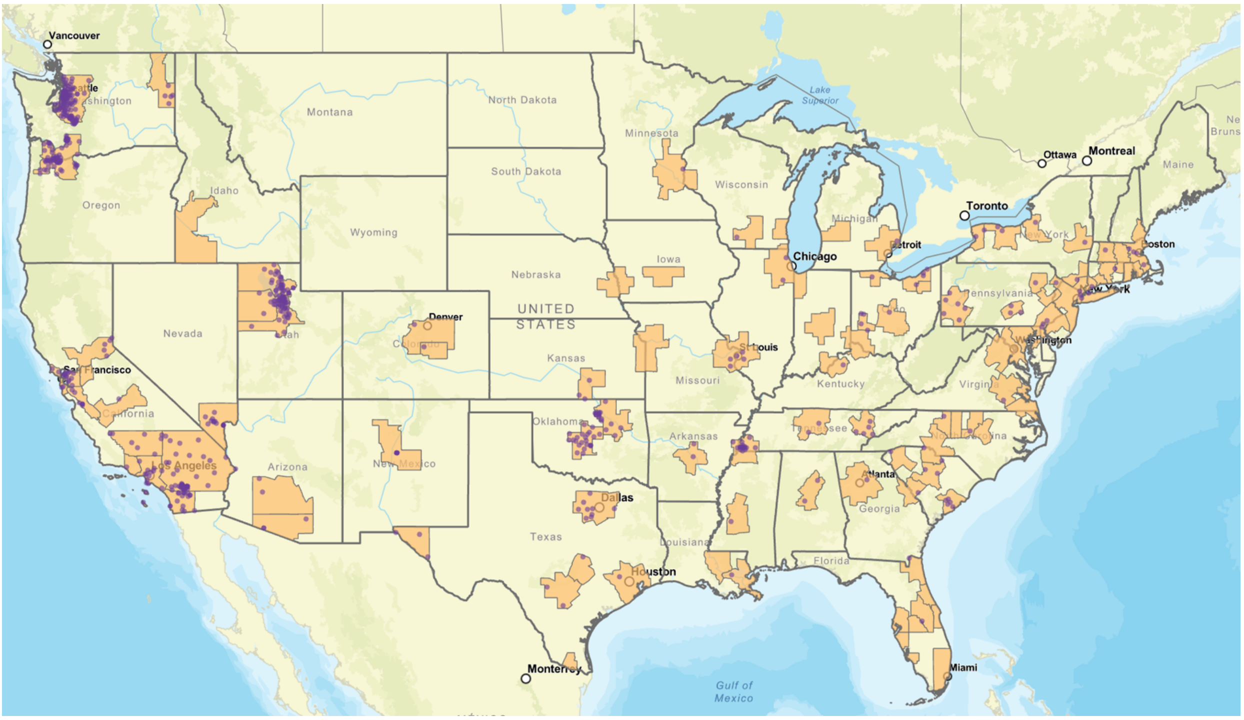

Figure 3: Geographic distribution of the 100 largest metropolitan statistical areas (MSAs) in the US (orange polygons) along with the active dedicated seismic sensors in each MSA (purple points).

Conducting spatial analysis

Our methodology uses average noise measurements to calculate the radius of the detection threshold for a single point or linearly distributed sensor, and then determine a buffer area around the sensor. Calculating the coverage of a set of sensors within an MSA requires a spatial analysis that accounts for the geographic location of sensors, the irregular perimeters of MSAs, as well as the extent of the sensor coverage area and its directivity. For this, we considered multiple layers of data to spatially understand relationships using a GIS. Specifically, we considered the following layers of data: fiber optic cable from Internet Atlas (linestring data), MSA perimeters from the US Census Bureau (multipolygons), location of ground motion sensors from IRIS (point data), and perimeters of detection areas – calculated using the methodology outlined above – for dedicated seismic sensors and fiber optic cable (multipolygons).

We identified the largest MSAs by population by joining two data sources from the US Census Bureau: the MSA geographic shapefile and a table of MSA populations US Census (2023). For each MSA, we then conducted spatial joins with the fiber optic cable and seismic sensor location shapefiles to identify the fiber and sensors within each MSA. The MSA extent and sensors within the 100 largest MSAs are shown in Figure 3.

For the fiber and sensors within an MSA, we used the detection threshold radius for M0.5 ground motion events to create layers with spatial buffers around each fiber segment and each sensor. The equations assume that the sensors have circular buffers created from variable-length detection threshold radii, while the fiber had irregular polygon buffers that followed the fiber route. Where detection threshold buffers exceeded the MSA perimeters, we spatially truncated the buffers to limit them to the spatial extent of the MSA polygon.

With the detection threshold buffers for dedicated seismic sensors as well as for fiber optic cable, we next determined the total coverage area within each MSA. We accounted for overlapping coverage areas in the following manner: we first spatially dissolved the sensor buffers to remove overlap in coverage, then we spatially dissolved the fiber optic cable buffers. Finally, we gave precedence to existing seismic sensor coverage area and we remove any overlapping coverage area from the fiber buffers. With the buffers thus prepared, we used the GIS to calculate the areas of the MSA, fiber buffer coverage, and point sensor buffer coverage.

One consideration with the total coverage area calculations described above is that they permit overlapping detection coverage without penalizing for sensors with overlapping coverage that does not improve the overall spatial coverage in the MSA. Deploying new sensing capabilities in fiber optic cables could be costly in terms of equipment required, labor costs to install, as well as in operating costs. Therefore, we needed a method to determine the largest coverage area while reducing the number of fiber optic cable segments that require installation of new sensing capabilities, a standard minimax problem. For this, we first spatially created the detection threshold buffers around each fiber optic cable segment and seismic sensor for an MSA, as described above. However, we maintained each detection threshold buffer around the fiber optic cable segments as a separate polygon shape and did not dissolve the polygons around each fiber segment into a single shape. In this manner, we determined the detection area around each fiber segment if we installed a sensing capability in that fiber optic cable segment.

Next, we spatially identified and removed any fiber detection buffer from consideration that overlapped with any point sensor buffer. Since dedicated seismic sensors are already in place and have been deliberately deployed, there is no increase of the spatial coverage area if additional sensing capability were deployed in a fiber optic cable in that area (although some point sensors could potentially be decommissioned in order to reduce operating costs). After removing these fiber detection buffers from consideration, we next took a greedy approach to identify the largest coverage area possible using the fewest number of new sensors in fiber optic cable. In general, a greedy algorithm is an iterative strategy that makes the locally optimal choice at each stage of the problem with the possibility of finding a global optimum. A greedy algorithm iteratively makes the best choice available at each step, based on a certain set of rules, and then moves on to the next step. The algorithm finishes when a stopping criterion has been met. Specifically, we sorted all fiber detection buffers that did not overlap with the dedicated sensor buffers from largest area to smallest and then iterated through each fiber buffer. We started with an empty set of optimal fiber detection coverage. At each step, if the fiber buffer under consideration did not overlap with any buffer in the optimal fiber detection coverage set, we added that buffer to the optimal fiber detection coverage set. In this manner, we significantly reduced the number of new sensors required for deployment on deployed fiber, while maintaining robust ground motion detection coverage throughout most MSAs. We demonstrate the effectiveness of this strategy in Section Results.

RESULTS

Spatial analysis of largest MSAs in the US

Of the top 100 MSAs considered in our analysis, the largest (New York-Newark-Jersey City) has a population of over 20 million people, while the smallest (Scranton–Wilkes-Barre, PA) has a population of just over 565K. The average population of the top 100 MSAs is 2.2M. Table 5 in the appendix shows the ten largest MSAs by population. By area, MSAs range in size from 71,000 km^2 (Riverside-San Bernardino-Ontario, CA) down to 1,600 km^2 (New Haven-Milford, CT), with an average area of 12,000 km^2.

Figure 3 shows the 100 largest MSAs along with the active dedicated seismic sensors within MSA boundaries. When considering currently deployed dedicated seismic sensors in the 100 largest MSAs, on average there are three sensors per MSA. There are 30 MSAs with no active dedicated seismic sensors. There are seven MSAs with ten or more active dedicated seismic sensors, enumerated in the appendix. Across all of the 100 largest MSAs, our analysis shows that on average, seismic sensors can detect low-magnitude ground motion events in 1% of an MSA's area. Albuquerque, NM has the most area covered by seismic sensors, with 2,800 km^2 (12%) of the land area covered by active dedicated sensors.

Recognizing that 30 of the 100 largest MSAs do not have any active seismic sensors, and that the MSAs with dedicated sensors can detect low-magnitude ground motion events in only about 1% of the total area, there is much opportunity to expand the sensor coverage area. If all fiber optic cable in each MSA were used as sensors, when considering low-magnitude (M0.5) ground motion events, our analysis shows that on average 19% of the MSA total area could be covered. New Haven-Milford, CT has the smallest area within which an event could be detected (54 km^2) by fiber optic cable sensors. This is only 3% of the total MSA area of 1,600 km^2. In contrast, by percentage of MSA covered, Cleveland-Elyria, OH has the largest area that could be covered by fiber optic cable sensors (40%). Atlanta-Sandy Springs-Alpharetta, GA has the next largest area that could be covered by fiber optic cable sensors: 8,600 km^2, which is 38% of the total MSA area (23,000 km^2).

Next, we assess how ground motion sensors deployed within existing fiber optic cable could *complement* dedicated seismic sensors. On average, a combination of dedicated seismic sensors and sensors using fiber optic cable could detect low-magnitude events in 2,200 km^2 (20%) of an MSA's total area. In the best case, Dallas-Fort Worth-Arlington, TX MSA has the largest area (11,300 km^2 or 49%) that could be covered by fiber optic cable and seismic sensors.

Because of the abundance of fiber optic cable in different MSAs that could harnessed for seismic sensing, it is important to identify the fewest fiber optic cable segments that provide the largest coverage area, *without overlapping coverage areas*. Using this technique, on average 1,400 km^2 (12%) of each county could be covered by either a fiber optic sensor or a dedicated seismic sensor.

Our results across all of the MSAs are summarized in Table 1. This shows that using sensors on fiber optic cable could improve the coverage area from 1% (using only dedicated seismic sensors) to almost 20% (using all fiber optic cable). In a more constrained fashion, using our optimal placement methodology, over 12% of an MSA would be covered by sensors on

Table 1. : Summary of area in the 100 largest MSAs within which low-magnitude seismic events (M0.5) could be detected using different combinations of ground motion sensors.

Sensor types	**Average area (km^2)**	**Percent of MSA area**
Existing seismic sensors	218	1.1%
Fiber optic cable	1,975	18.7%
Fiber and seismic sensors	2,194	19.8%
Optimal fiber and seismic sensors	1,383	12.2%

a minimal selection of fiber optic cable alongside dedicated seismic sensors. See Table 6 in the appendix for a list of results for the top 75 MSAs.

Spatial analysis of Little Rock, AR

Focusing attention on a specific MSA allows us to better understand the spatial relationships of an MSA in which low-magnitude ground motion events could be detected by dedicated seismic sensors, by sensors deployed on fiber optic cable, and by sensors only placed in an optimal fashion within fiber optic cable.

We chose Little Rock, AR for our first case study because of its proximity to the New Madrid Seismic Zone (NMSZ) Missouri Department of Natural Resources (2023) and because of the illustrative characteristics of seismic sensors and fiber optic cable in the MSA. The NMSZ is a region in the central United States, spanning parts of Missouri, Arkansas, Tennessee, Kentucky, and Illinois where a high level of seismic activity has been recorded. Because the NMSZ is one of the most active seismic zones in the central and eastern United States with the potential to damage heavily populated areas, it is closely monitored by the United States Geological Survey (USGS) (2023). Because large magnitude earthquakes are infrequent, structures are not always consistent with the latest seismic building codes. Therefore, damage from a large magnitude event could be extremely costly. Ambient noise tomography, using improved sensing coverage and traffic as a noise source, can be used to obtain near-surface shear-velocity profiles and to compute engineering parameters such as VS30, the average shear-wave velocity in the top 30 meters. This can help to define which areas are the most vulnerable.

The Little Rock, AR MSA includes the city of Little Rock and the surrounding area, including Pulaski County, covering 10,933 km^2. There are two active dedicated seismic sensors in the MSA, shown as green dots in Figure 4. The Woolly Hollow State Park, AR sensor (WHAR) from the Arkansas seismic sensor network is located in the northern part of the MSA, and the University of Arkansas, Little Rock sensor (UALR) from the New Madrid (NM) seismic sensor network is located near the center of the MSA in city of Little Rock.

Using the noise measurements described in Section Datasets, we calculated the maximum distance from each sensor in which a low-magnitude ground motion event could be detected. Because of high noise around the UALR sensor, the detection radius was less than 0.5 km. However, the WHAR sensor had much lower noise at the sensor site and, therefore, could detect low-magnitude seismic events in the 704 km^2 surrounding the sensor, as represented by the purple circle in Figure 4. This results in 6.5% of the Little Rock MSA having coverage from dedicated seismic sensors for low-magnitude events.

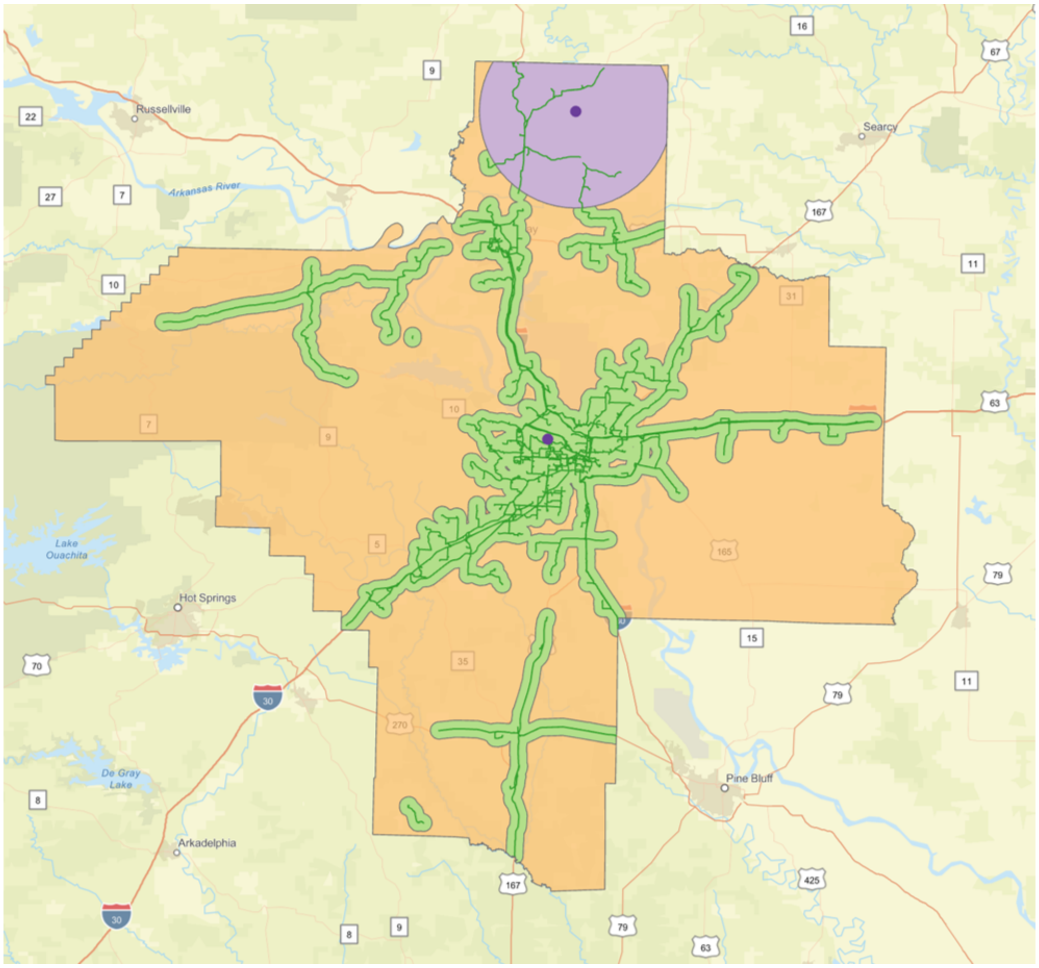

Figure 4: Geographic extent of the Little Rock, AR MSA (orange polygon) with existing dedicated seismic sensor coverage for low-magnitude events (purple buffer), existing ISP fiber optic cables (green lines), and *potential* detection area for low-magnitude ground motion events using fiber optic cable as sensors (light green buffer).

The fiber network in the Little Rock MSA, depicted by the green lines in Figure 4, is quite extensive. The center of the MSA is the city of Little Rock, with metropolitan fiber throughout the city. Long haul fiber then runs from Little Rock to the north, east, and south along Interstate highways I40, I30, and I530 to smaller cities and towns, including Conway, Bryant, and Pine Bluff. We are not aware of any ground motion sensors currently deployed using the fiber optic network, so we cannot collect existing noise measurements with which to calculate the buffer along each cable within which ground motion events could be detected. We therefore assume a high noise level around the fiber optic cable, and assume that the cable can be used to uniformly detect ground motion events of M0.5 within 1.5 km of the cable. Of note is that some of the possible coverage from using sensors on fiber optic cable in the northern part of the MSA would overlap with seismic sensor coverage already in place. We explicitly removed all fiber optic coverage buffers that overlapped with existing seismic sensor coverage from consideration, with the expectation that any deliberately placed seismic sensor would provide more robust ground motion detection than that placed using ISP fiber optic cable. Our results show that 2,565 km^2 (23.5%) of the MSA is within the low-

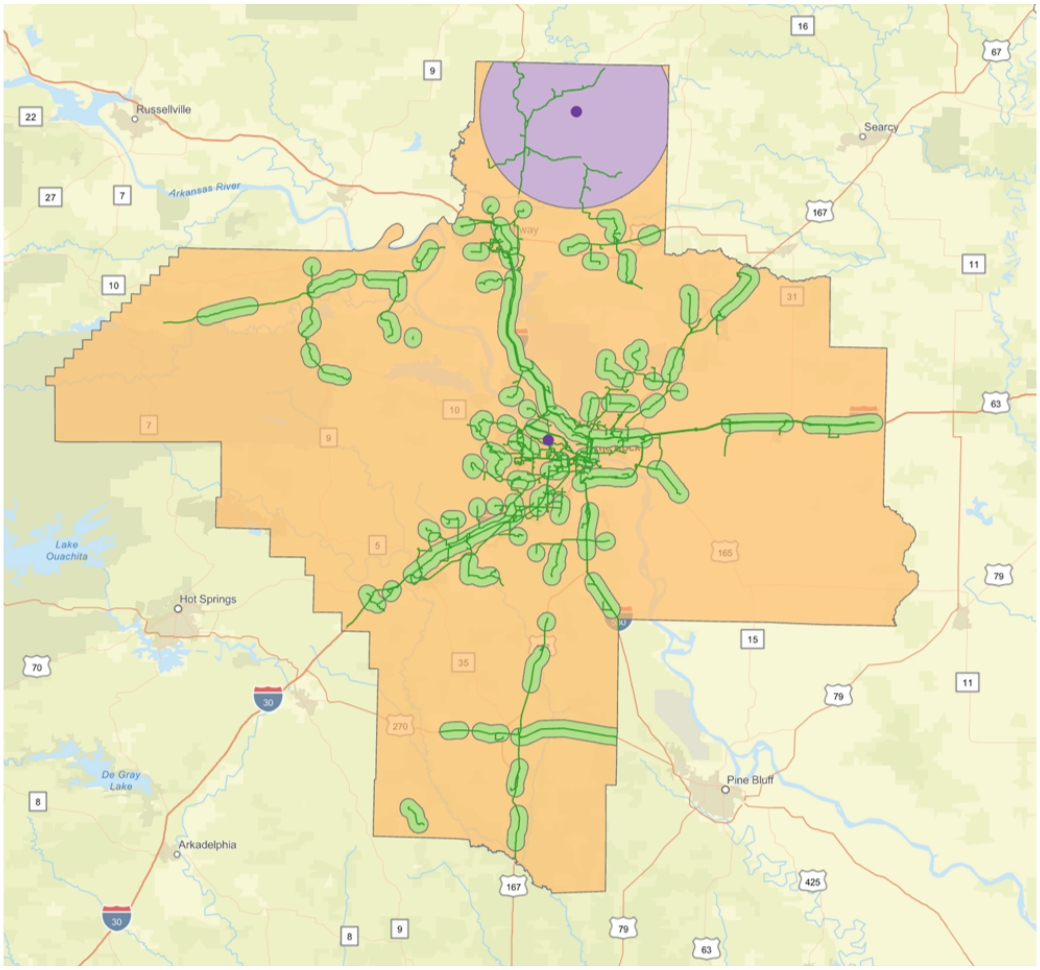

Figure 5: Geographic extent of the Little Rock, AR MSA (orange polygon) with existing dedicated seismic sensor coverage for low-magnitude events (purple buffer), existing ISP fiber optic cables (green lines), and *optimal* detection area for low-magnitude ground motion events using fiber optic cable as sensors (light green buffer).

magnitude ground motion event detection threshold if all fiber optic cable was used for event detection. If both deployed point sensors and fiber-based sensors were used, coverage would expand to 3,259 km^2 (30%) of the MSA.

However, this is an optimistic scenario that would require extensive resources to be deployed along many different fiber optic segments and would result in a great deal of overlapping coverage without added spatial coverage. We therefore used the optimal analysis algorithm described in Section Methodology to determine that using only 72 of the 2,452 fiber optic cable segments in the MSA could provide detection coverage of 1,407 km^2 (12.9% of the MSA). As shown in Figure 5, using this optimal number of fiber optic cables provides 55% coverage of the total possible area using fewer than 2.9% of fiber segments. We summarized these results in Table 2.

Spatial analysis of Seattle, WA

In contrast to the Little Rock MSA, the Seattle MSA is an area in which point sensors are much more widely deployed so selection to extend the coverage area would have to be considered more carefully. The Seattle, WA MSA covers 15,535 km^2

Table 2. : Area of Little Rock MSA within which low-magnitude seismic events (M0.5) could be detected using different combinations of ground motion sensors.

Sensor types	MSA area (km^2)	Percent of MSA area
Existing seismic sensors	704	6.5%
Fiber optic cable	2,565	23.5%
Fiber and seismic sensors	3,259	30%
Optimal fiber and seismic sensors	2,107	19.4%

and encompasses the cities of Seattle, Tacoma and Bellevue, as well as the surrounding commercial and industrial areas, and smaller communities.

There are 27 seismic sensing stations in the MSA, with most of the sensors outside of the major urban areas in the southeast area of the MSA. These sensors can be used to detect low-magnitude ground motion events over 1,005 km^2, which amounts to 6.5% of the MSA. As seen by the purple circles in Figure 6, many of the sensors are placed close proximity, providing overlapping coverage areas. As a demonstration of these sensors' ability to detect anthropogenic ground motion events, one

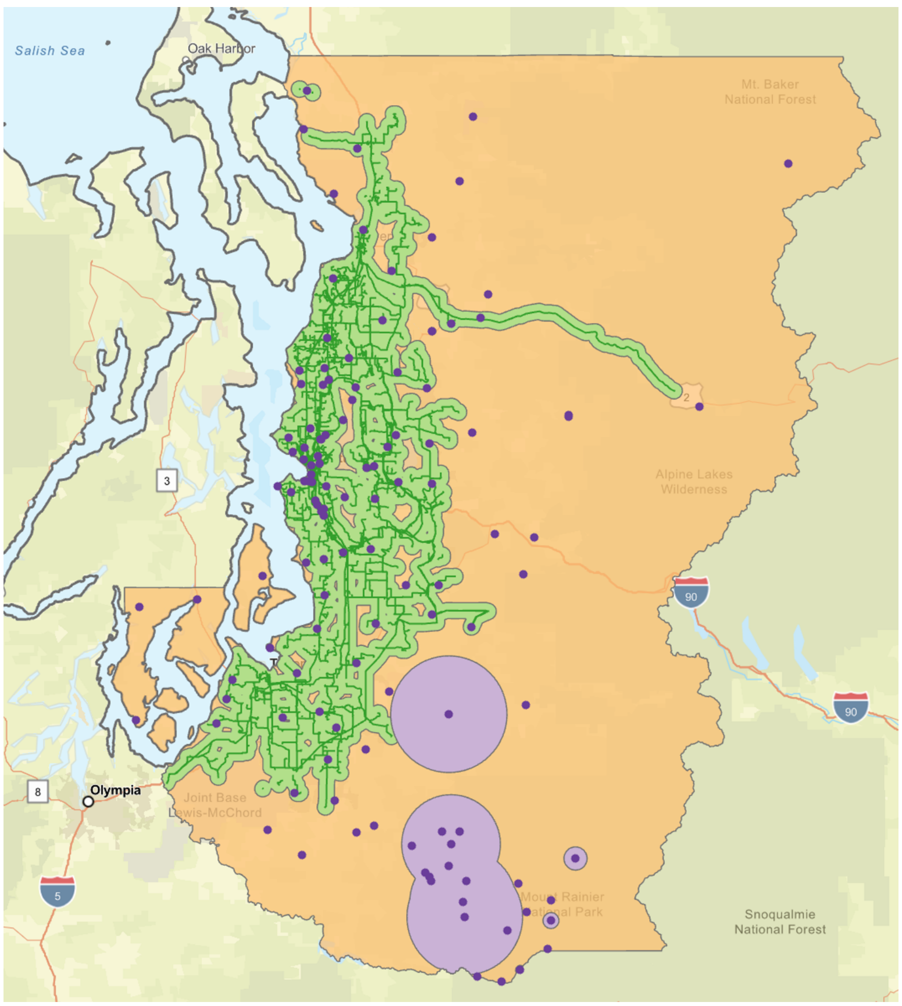

Figure 6: Geographic extent of the Seattle, WA MSA (orange polygon) with existing dedicated seismic sensor coverage for low-magnitude events (purple buffers), existing ISP fiber optic cables (green lines), and *potential* detection area for low-magnitude ground motion events using fiber optic cable as sensors (light green buffer).

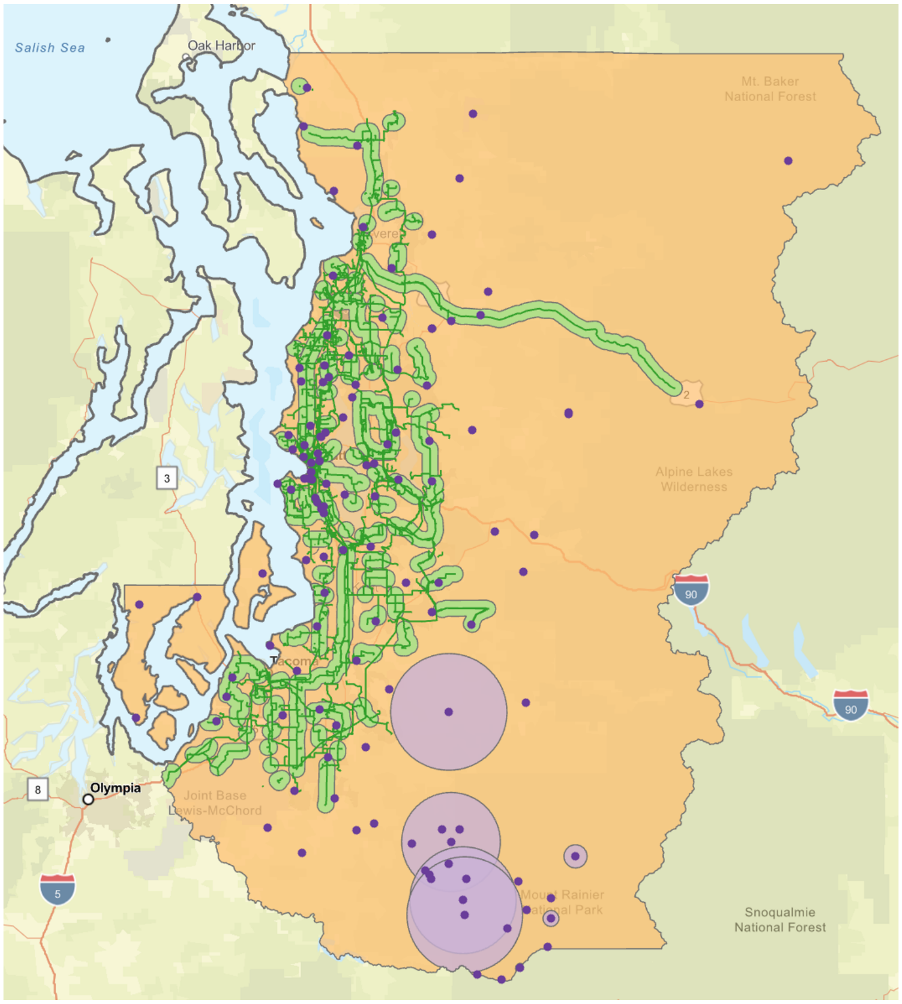

Figure 7: Geographic extent of the Seattle, WA MSA (orange polygon) with existing dedicated seismic sensor coverage for low-magnitude events (purple buffers showing overlapping coverage area), existing fiber optic cables (green lines), and *optimal* detection area for low-magnitude ground motion events using fiber optic cable as sensors (light green buffer).

of these sensors which is deployed in a large stadium (Kingdome, Seattle, WA – KDK) detected crowd noise during a sporting event in 2011 Vidale (2011).

Similar to the dedicated sensors, much of the fiber optic cable is located along the western part of the Seattle MSA. This reinforces our premise that, because fiber is deployed in areas where people live, it offers a compelling for use in ground motion sensing in a smart city. For low-magnitude ground motion events, if sensors were deployed over the entire fiber network, the total area in which ground motion events could be detected is 3,046 km^2, which is 19.61% of the Seattle MSA.

It is important to note that much of this MSA is, in fact, rural, and the coverage in populated areas is much higher. Furthermore, since almost all of the current seismic sensor coverage area is *outside* of the area that could be covered by sensors using fiber optic cable, those sensors would significantly extend the coverage area throughout the MSA – especially in densely populated urban areas. All dedicated seismic sensors and possible sensors in fiber optic cable would cover 4,052 km^2 (26.1%) of the entire MSA for low-magnitude events.

Table 3. : Area of Seattle-Tacoma-Bellevue MSA within which low-magnitude seismic events (M0.5) could be detected using different combinations of ground motion sensors.

Sensor types	**MSA area (km^2)**	**Percent of MSA area**
Existing seismic sensors	1,005	6.5%
Fiber optic cable	3,046	19.6%
Fiber and seismic sensors	4,052	26.1%
Optimal fiber and seismic sensors	2,868	18%

More conservatively, if we consider the scenario in which we only deploy new sensors on fiber optic cable in a manner in which the coverage area does not overlap, we still find significant gain as compared to only using currently-deployed dedicated seismic sensors. As depicted in Figure 7, optimal placement of sensors using fiber optic cable would provide non-overlapping coverage of 1,862 km^2 (12%) of the MSA. In this case, optimal placement means using our greedy approach to install sensing capability on only 74 of the 16,052 total fiber segments (0.5%) in the MSA. Considering the total coverage area of optimal sensors using fiber optic cable in addition to the existing sensor coverage area, we see 2,868 km^2 (18%) of the MSA covered for low-magnitude ground motion events. These results are summarized in Table 3.

DISCUSSION

While we are not aware of any instances of ground motion sensors that have been permanently deployed on ISP fiber optic cables, our results highlight tantalizing opportunities for smart cities and for equipment manufacturers. In particular, our methodology enables city planners to assess and manage ground motion sensing coverage while minimize deployment costs. Similarly, there has been a groundswell of companies developing DAS devices (*e.g.,* Silixa (2023); Optasense (2023)) over the past several years. While there are compelling applications in commercial areas, our methodology and results can be used to motivate configurations for deployment for urban ground motion monitoring.

Our calculations for the ground motion detection coverage area for each fiber segment is a conservative estimate since as far as we know, there have been no studies of ambient noise for DAS deployed on ISP fiber optic cables. More accurate noise measurements on fiber optic cable segments would improve the accuracy of detection thresholds. With the noise measurements that we consider for point sensors, we average across a 24 hour period. While we believe this is reasonable for our study, noise estimation could be more broadly considered using historical measurements from deployed sensors.

Finally, we used fiber optic cable maps from from Internet Atlas Durairajan et al. (2013), which are the most accurate maps available for research and include data for over 200 MSAs in the US. However, these maps may not represent all fiber segments for all ISPs that operate in the top 100 MSAs. ISPs consistently deploy new optical fiber to improve the speed and reliability of their services. While ISPs are typically reticent to share details of their infrastructures for competitive reasons, coverage analysis would be improved with the most comprehensive and up-to-date maps of fiber infrastructure deployments.

CONCLUSION

In this paper, we assess the possible expansion of area monitored for ground motion if ISP fiber optic cables were used for sensing. We found that the abundance of fiber optic cable in metropolitan areas offers significant opportunity to extend the ground motion event detection coverage area of the 100 largest metropolitan service areas in the US. Our method for conducting this analysis utilizes GIS to model layers of ground motion detection coverage from existing point sensors and hypothetical fiber-based linearly distributed sensors inside the boundaries of metropolitan areas. Our analysis of the top 100 MSAs showed that, on average, ISP fiber optic cable used as ground motion sensors could cover 18.7% of an MSA. Even when deployed in an optimal fashion to mimimize costs, ISP fiber optic cable used as sensors and existing seismic sensors could cover 12.2% of an MSA – an order of magnitude increase over what can be covered with existing seismic sensors. In two case studies of Little Rock, AR and Seattle, WA we showed that, even in MSAs with multiple seismic sensors, new sensors placed using fiber optic cable could extend the ground motion event detection area, which would provide exciting opportunities to monitor anthropogenic industrial, economic, and transportation activity in smart cities. Improved ground motion detection in smart cities could be used to improve public safety, infrastructure management, emergency response and our understanding of longer term issues like anthropogenic responses to climate change.

DATA AND RESOURCES

All data used in this paper came from published sources listed in the references.

ACKNOWLEDGEMENTS

FIXME: This work is supported by National Science Foundation (NSF) grants CNS-1703592, CNS-2039146. The views and conclusions contained herein are those of the authors and should not be interpreted as necessarily representing the official policies or endorsements, either expressed or implied, of NSF or the U.S. Government. The authors declare no competing interests.

REFERENCES

Aazam, M., M. St-Hilaire, C.-H. Lung, and I. Lambadaris (2016). Cloud-based smart waste management for smart cities. In *2016 IEEE 21st International Workshop on Computer Aided Modelling and Design of Communication Links and Networks (CAMAD)*, pp. 188–193.

Adedeji, K. B., A. A. Ponnle, A. M. Abu-Mahfouz, and A. M. Kurien (2022). Towards digitalization of water supply systems for sustainable smart city development – water 4.0. *Applied Sciences* **12**(18).

Ajo-Franklin, J. B., S. Dou, N. J. Lindsey, I. Monga, C. Tracy, M. Robertson, V. Rodriguez Tribaldos, C. Ulrich, B. Freifeld, T. Daley, and X. Li (2019). Distributed acoustic sensing using dark fiber for near-surface characterization and broadband seismic event detection. *Scientific Reports* **9**(1), 2045–2322.

Allen, R., P. Gasparini, O. Kamigaichi, and M. Bose (2009). The Status of Earthquake Early Warning around the World: An Introductory Overview. *Seismological Research Letters* **80**(5), 682–693.

Argany, M., M. Mostafavi, F. Karimipour, and C. Gagné (2011). A GIS Based Wireless Sensor Network Coverage Estimation and Optimization: A Voronoi Approach. *Transactions on Computational Science XIV* **6970**.

Cascone, V., J. Boaga, and G. Cassiani (2021). Small local earthquake detection using low-cost mems accelerometers: Examples in northern and central italy. *The Seismic Record* **1**(1), 20–26.

Cunningham, E., N. Lord, D. Fratta, H. F. Wang, J. Catudal, and P. R. Barford (2022, December). Characterizing Dark Fiber DAS along a University Campus Route. In *AGU Fall Meeting Abstracts*, Volume 2022, pp. S12D–0180.

Durairajan, R., S. Ghosh, X. Tang, P. Barford, and B. Eriksson (2013). Internet atlas: A geographic database of the internet. In *Proceedings of the 5th ACM Workshop on HotPlanet*, New York, NY, USA, pp. 15–20. Association for Computing Machinery.

D'Aniello, G., M. Gaeta, F. Orciuoli, G. Sansonetti, and F. Sorgente (2020). Knowledge-based smart city service system. *Electronics* **9**(6).

Esri (2020). Esri ArcGIS. https://www.esri.com/.

Fu, J., Z. Li, H. Meng, J. Wang, and X. Shan (2019). Performance evaluation of low-cost seismic sensors for dense earthquake early warning: 2018–2019 field testing in southwest china. *Sensors* **19**(9), 1999.

GeoPandas (2023). GeoPandas. https://geopandas.org/.

IRIS Consortium (2023). IRIS Gmap. https://ds.iris.edu/gmap/.

Kirimtat, A., O. Krejcar, A. Kertesz, and M. Tasgetiren (2020). Future trends and current state of smart city concepts: A survey. *IEEE Access* **8**, 86448–86467.

Kong, Q., R. M. Allen, L. Schreier, and Y.-W. Kwon (2016). Myshake: A smartphone seismic network for earthquake early warning and beyond. *Science Advances* **2**(2), e1501055.

Krokidis, S., I. Vlachos, M. Avlonitis, A. Kostoglou, and V. Karakostas (2022). Data-driven performance evaluation of a low-cost seismograph. *Measurement and Control* **55**(5-6), 340–358.

Lindsey, N. J., E. R. Martin, D. S. Dreger, B. Freifeld, S. Cole, S. R. James, B. L. Biondi, and J. B. Ajo-Franklin (2017). Fiber-optic network observations of earthquake wavefields. *Geophysical Research Letters* **44**(23), 11–792.

Lindsey, N. J., S. Yuan, A. Lellouch, L. Gualtieri, T. Lecocq, and B. Biondi (2020). City-scale dark fiber das measurements of infrastructure use during the covid-19 pandemic. *Geophysical Research Letters* **47**(16), e2020GL089931.

Mahapatra, C., A. K. Moharana, and V. C. M. Leung (2017). Energy management in smart cities based on internet of things: Peak demand reduction and energy savings. *Sensors* **17**(12).

Malekloo, A., E. Ozer, and F. Al-Turjman (2020). *Smart Grid in IoT-Enabled Spaces*, Chapter Combination of GIS and SHM in Prognosis and Diagnosis of Bridges in Earthquake-Prone Locations. CRC Press.

Martin, E. R., C. M. Castillo, S. Cole, P. S. Sawasdee, S. Yuan, R. Clapp, M. Karrenbach, and B. L. Biondi (2017). Seismic monitoring leveraging existing telecom infrastructure at the SDASA: Active, passive, and ambient-noise analysis. *The Leading Edge* **36**(12), 1025–1031.

Missouri Department of Natural Resources, M. D. (2023). Facts about the New Madrid Seismic Zone. https://dnr.mo.gov/land-geology/hazards/earthquakes/science/facts-new-madrid-seismic-zone.

Nirde, K., P. S. Mulay, and U. M. Chaskar (2017). Iot based solid waste management system for smart city. In *2017 International Conference on Intelligent Computing and Control Systems (ICICCS)*, pp. 666–669.

Observatory, U. H. V. (2008). Volcano Watch — What was that on the Richter scale? https://www.usgs.gov/observatories/hvo/news/volcano-watch-what-was-richter-scale.

Optasense (2023). Distributed Acoustic Sensing Interrogators. https://www.optasense.com/.

Parker, T., S. Shatalin, and M. Farhadiroushan (2014). Distributed acoustic sensing–a new tool for seismic applications. *first break* **32**(2).

Patnaik, S., P. Barford, D. Fratta, B. Jensen, N. Lord, M. Malloy, and H. Wang (2021). Internet photonic sensing: Using internet fiber optics for vibration measurement and monitoring. *Proceedings of the ACM SIGCOMM Workshop on Optical Systems (OptSys)*.

Reilly, J., S. Dashti, M. Ervasti, J. D. Bray, S. D. Glaser, and A. M. Bayen (2013). Mobile phones as seismologic sensors: Automating data extraction for the ishake system. *IEEE Transactions on Automation Science and Engineering* **10**(2), 242–251.

Rizwan, P., K. Suresh, and M. R. Babu (2016). Real-time smart traffic management system for smart cities by using internet of things and big data. In *2016 International Conference on Emerging Technological Trends (ICETT)*, pp. 1–7.

Shen, J. and T. Zhu (2021). Seismic Noise Recorded by Telecommunication Fiber Optics Reveals the Impact of COVID-19 Measures on Human Activity. *The Seismic Record* **1**(1), 46–55.

Silixa (2023). iDAS - intelligent Distributed Acoustic Sensor. https://www.silixa.com/.

United States Census Bureau (2023). Cartographic Boundary Files - Shapefiles. https://www.census.gov/geographies/mapping-files/time-series/geo/carto-boundary-file.html.

United States Census Bureau (2023). Metropolitan and Micropolitan Statistical Areas Population Totals and Components of Change: 2020-2021. https://www.census.gov/data/tables/time-series/demo/popest/2020s-total-metro-and_micro-statistical-areas.html.

United States Geological Survey (USGS) (2023). The New Madrid Seismic Zone. https://www.usgs.gov/programs/earthquake-hazards/new-madrid-seismic-zone.

USGS Earthquake Hazards Program (2023). Earthquake Magnitude, Energy Release, and Shaking Intensity. https://www.usgs.gov/programs/earthquake-hazards/earthquake-magnitude-energy-release-and_shaking-intensity.

Vidale, J. E. (2011, 05). Seattle "12th Man* Earthquake" Goes Viral. *Seismological Research Letters* **82**(3), 449–450.

Wang, H. F., X. Zeng, D. E. Miller, D. Fratta, K. L. Feigl, C. H. Thurber, and R. J. Mellors (2018). Ground motion response to an ml 4.3 earthquake using co-located distributed acoustic sensing and seismometer arrays. *Geophysical Journal International* **213**(3), 2020–2036.

Wilson, D. C., E. Wolin, W. L. Yeck, R. E. Anthony, and A. T. Ringler (2021, 10). Modeling Seismic Network Detection Thresholds Using Production Picking Algorithms. *Seismological Research Letters* **93**(1), 149–160.

Working Group on Instrumentation, Siting, Installation, and Site Metadata (2008). Instrumentation guidelines for the advanced national seismic system: U.S. Geological Survey. *Open-File Report 2008–1262*.

Wuestefeld, A. and M. Wilks (2019). How to twist and turn a fiber: Performance modeling for optimal das acquisitions. *The Leading Edge* **38**(3), 226–231.

Zhu, T., J. Shen, and E. R. Martin (2021). Sensing earth and environment dynamics by telecommunication fiber-optic sensors: an urban experiment in pennsylvania, usa. *Solid Earth* **12**(1), 219–235.

Appendix

Section Calculating detection threshold described our methodology to calculate detection thresholds from noise measurements. For reference, we reproduced the coefficients for equations 1, 2, and 3 for P-waves calculated by Wilson et al. (2021) in Table 4.

Table 4. : Coefficients for noise versus distance for equations 1, 2, and 3 from Wilson et al. (2021).

Coefficient	P-Wave Value	Units
r_1	$9.04x10^1$	km
r_2	$3.35x10^2$	km
a_1	$9.26x10^{-2}$	M/km
a_2	-3.85	M/km
a_3	$9.69x10^{-1}$	M/km
b_1	$1.03x10^{-2}$	M/km
b_2	$1.46x10^{-2}$	M/dB
d	$2.60x10^{-2}$	M/dB
c	3.95	Magnitude (M)

Section Spatial analysis of largest MSAs in the US described our analysis of the 100 largest MSAs. Table 5 shows the ten largest MSAs by population.

Table 5. : Largest MSAs in the US (by population).

MSA Name	States	Population (millions)
New York-Newark-Jersey City	NY-NJ-PA	20.3
Los Angeles-Long Beach-Anaheim	CA	13.3
Chicago-Naperville-Elgin	IL-IN-WI	9.7
Dallas-Fort Worth-Arlington	TX	7.5
Houston-The Woodlands-Sugar Land	TX	7.0
Philadelphia-Camden-Wilmington	PA-NJ-DE-MD	6.1
Washington-Arlington-Alexandria	DC-VA-MD-WV	6.1
Miami-Fort Lauderdale-West Palm Beach	FL	6.1
Atlanta-Sandy Springs-Roswell	GA	6.0
Boston-Cambridge-Newton	MA-NH	4.9

There are seven MSAs with ten or more active dedicated seismic sensors:

- Riverside-San Bernardino-Ontario CA (47 sensors)
- Portland-Vancouver-Hillsboro OR-WA (33 sensors)
- Seattle-Tacoma-Bellevue WA (27 sensors)
- Oklahoma City OK (21 sensors)
- Tulsa OK (17 sensors)
- Los Angeles-Long Beach-Anaheim CA (12 sensors)
- Albuquerque NM (10 sensors)

Table 6. : Comparison of MSA coverage areas for the top 75 MSAs with most potential total detection area (including from existing seismic sensors and sensors using fiber optic cable) for low-magnitude (M0.5) ground motion events.

MSA Name	States	MSA Area (km^2)	Existing Sensors Area (km^2)	All Fiber Area (km^2)	Fiber and Sensors Area (km^2)	Optimal Fiber and Sensors Area (km^2)
Dallas-Fort Worth-Arlington	TX	23,332	2,713	8,642	11,356	6,828
Atlanta-Sandy Springs-Alpharetta	GA	22,899	0	8,646	8,646	5,103
Minneapolis-St. Paul-Bloomington	MN-WI	19,462	0	7,243	7,243	4,123
Riverside-San Bernardino-Ontario	CA	70,955	2,496	3,974	6,470	4,512
Chicago-Naperville-Elgin	IL-IN-WI	18,906	0	6,461	6,461	3,997
New York-Newark-Jersey City	NY-NJ-PA	19,048	6	6,292	6,298	3,647
Philadelphia-Camden-Wilmington	PA-NJ-DE-MD	12,285	0	6,179	6,179	3,762
Pittsburgh	PA	13,832	0	5,800	5,801	3,197
Washington-Arlington-Alexandria	DC-VA-MD-WV	17,429	0	5,228	5,228	3,147
Houston-The Woodlands-Sugar Land	TX	22,255	0	4,497	4,497	2,312
Charlotte-Concord-Gastonia	NC-SC	14,787	0	4,303	4,303	2,599
Las Vegas-Henderson-Paradise	NV	20,880	2,739	1,537	4,276	3,522
Detroit-Warren-Dearborn	MI	10,415	0	4,231	4,231	2,511
Miami-Fort Lauderdale-Pompano Beach	FL	14,159	0	4,168	4,168	2,656
Seattle-Tacoma-Bellevue	WA	15,535	1,006	3,046	4,052	2,868
Indianapolis-Carmel-Anderson	IN	11,235	0	3,927	3,927	2,445
Albuquerque	NM	24,068	2,818	1,003	3,821	3,150
Phoenix-Mesa-Chandler	AZ	37,797	0	3,474	3,474	2,234
Denver-Aurora-Lakewood	CO	21,746	463	3,007	3,470	2,268
Los Angeles-Long Beach-Anaheim	CA	12,677	141	3,321	3,462	1,905
Cleveland-Elyria	OH	5,215	0	3,446	3,446	2,081
Omaha-Council Bluffs	NE-IA	11,423	0	3,404	3,404	2,013
Ogden-Clearfield	UT	22,357	2,752	651	3,403	3,177
Des Moines-West Des Moines	IA	9,434	0	3,385	3,385	2,085
Salt Lake City	UT	20,961	2,033	1,319	3,352	2,831
Kansas City	MO-KS	19,089	0	3,294	3,294	2,039
Columbus	OH	12,560	0	3,271	3,271	1,957
Little Rock-North Little Rock-Conway	AR	10,868	704	2,555	3,259	2,107
Nashville-Davidson–Murfreesboro–Franklin	TN	14,922	0	3,154	3,154	1,844
St. Louis	MO-IL	20,944	0	2,598	2,598	1,826
Cincinnati	OH-KY-IN	11,999	0	2,508	2,508	1,635
Richmond	VA	11,629	0	2,442	2,442	1,480
Memphis	TN-MS-AR	12,163	0	2,436	2,436	1,463
Louisville/Jefferson County	KY-IN	8,521	50	2,330	2,380	1,377
Birmingham-Hoover	AL	11,813	209	2,143	2,352	1,428
San Francisco-Oakland-Berkeley	CA	6,627	8	2,322	2,330	1,254
Tulsa	OK	16,745	1	2,264	2,264	1,358
Virginia Beach-Norfolk-Newport News	VA-NC	9,783	0	2,204	2,204	1,224
San Diego-Chula Vista-Carlsbad	CA	11,019	1,175	905	2,080	1,839
Toledo	OH	4,248	0	1,870	1,870	1,060
Jacksonville	FL	8,866	0	1,819	1,819	1,061
Portland-Vancouver-Hillsboro	OR-WA	17,662	229	1,554	1,783	1,176
Oklahoma City	OK	14,452	0	1,747	1,747	1,209
Baltimore-Columbia-Towson	MD	7,015	0	1,730	1,730	887
San Antonio-New Braunfels	TX	19,076	7	1,681	1,688	1,015
Tampa-St. Petersburg-Clearwater	FL	6,936	0	1,655	1,655	1,029
Deltona-Daytona Beach-Ormond Beach	FL	4,590	0	1,532	1,532	1,017
Provo-Orem	UT	14,366	825	648	1,472	1,038
Winston-Salem	NC	5,281	0	1,458	1,458	861
Austin-Round Rock-Georgetown	TX	11,075	0	1,415	1,415	880
Madison	WI	8,773	1	1,395	1,396	975
Grand Rapids-Kentwood	MI	7,119	0	1,383	1,383	888
Milwaukee-Waukesha	WI	3,866	0	1,344	1,344	800
Spokane-Spokane Valley	WA	11,184	802	531	1,333	1,124
Akron	OH	2,392	0	1,333	1,333	778
El Paso	TX	14,460	239	1,090	1,329	850
Sacramento-Roseville-Folsom	CA	13,743	30	1,285	1,315	779
Boston-Cambridge-Newton	MA-NH	9,501	7	1,302	1,309	937
Wichita	KS	10,828	0	1,257	1,257	741
Harrisburg-Carlisle	PA	4,310	8	1,234	1,242	692
Orlando-Kissimmee-Sanford	FL	10,381	0	1,226	1,226	756
Greenville-Anderson	SC	7,216	0	1,220	1,220	442
Worcester	MA-CT	5,443	3	1,204	1,207	717
Syracuse	NY	6,433	1	1,176	1,177	676
Allentown-Bethlehem-Easton	PA-NJ	3,818	0	1,144	1,144	677
Columbia	SC	9,922	2	1,080	1,081	641
Tucson	AZ	23,790	235	842	1,077	720
Augusta-Richmond County	GA-SC	9,273	0	1,056	1,056	573
Cape Coral-Fort Myers	FL	2,299	0	1,026	1,026	668
Scranton–Wilkes-Barre	PA	4,598	0	1,018	1,018	548
Knoxville	TN	8,677	6	939	946	593
Dayton-Kettering	OH	3,344	0	891	891	507
Boise City	ID	30,629	0	873	873	564
Albany-Schenectady-Troy	NY	7,450	0	848	848	483
San Jose-Sunnyvale-Santa Clara	CA	6,967	33	784	817	473